

Raman identification of ancient stained glasses and their degree of deterioration

Philippe Colomban,^{1*} Marie-Pierre Etcheverry,² Magali Asquier,¹ Mathieu Bounichou¹ and Aurélie Tournié¹

¹ Laboratoire de Dynamique, Interaction et Réactivité (LADIR), UMR 7075 Centre National de la Recherche Scientifique & Université Pierre et Marie Curie, 2 rue Henri Dunant, 94320 Thiais, France

² Laboratoire de Recherche des Monuments Historiques (LRMH), 29 rue de Paris, 77420 Champs-sur-Marne, France

Received 10 August 2005; Accepted 18 November 2005

The aim of this investigation was to establish a Raman procedure for on-site identification of stained-glass windows and their deterioration level. This study of a representative series of stained-glass pieces dating from the thirteenth to seventeenth, nineteenth and twenty-first centuries made it possible to classify the glasses into four types: Type 1 (rare, Ca-rich Na silicate), Type 2 (rare, Na-rich, Ca silicate), Type 3 (more frequent, K–Ca silicate) and a variant of Type 3, referred to as 3bis. Ion exchange of the alkali cations was made in boiling sulfuric acid and related to structural and compositional changes, which were analyzed with IR and Raman spectroscopy, optical microscopy and EDS. Measurements of the film thickness showed a great discrepancy between the ion-exchange rates of K–Ca (Type 3: 60 $\mu\text{m}/\text{h}$) and Na–Ca (Type 2: 15 $\mu\text{m}/\text{h}$) silicates with that of Type 1 Ca-silicate (0.05 $\mu\text{m}/\text{h}$). IR and Raman spectra provided proof that the nanostructure of the glass was modified, chiefly by the downward (Raman) and upward (IR) shift of the position of the main Si–O stretching peak and a decrease in the intensity of the Boson peak, as well as the Raman 580 cm^{-1} Si–O bending peak. The decrease in intensity of the narrow $\sim 950 \text{ cm}^{-1}$ Raman peak, assigned to (earth)alkali nano crystallites in the glassy network, is correlated with the K/Na ion loss and glass weathering. Consequently Type 3bis samples are in fact glasses, in which the surface is depleted of K/Na ions. Optical micrographs support the macroscopic compositional and structural heterogeneity of the ancient glasses. This work demonstrates the potential of Raman scattering for *in situ* measurements of the degree of weathering of ancient stained glasses. Copyright © 2006 John Wiley & Sons, Ltd.

KEYWORDS: glass; silicate; conservation; vibrational spectroscopy; weathering; stained-glass window

INTRODUCTION

The weathering of stained-glass windows of ancient churches and cathedrals results in color changes and in some instances even severe physical damage.^{1–15} The environment to which the glass is exposed greatly influences the deterioration rate, and even museum conservation wood cases promote the deterioration of glass items.¹⁶ Alteration of the glass is attributed to a reaction between the glass surface and aqueous solutions in a two-stage process.^{6–15} The first stage is an ion-exchange process between protonic species from the liquid on the surface and an alkali ion that is removed from the glass, and results in the formation of an alkaline wet film on the surface. This film becomes increasingly

alkaline, and above pH 9, the second stage occurs with decomposition of the silica network. As a nondestructive technique, Raman spectroscopy has proved its potential in the analysis of the structure of amorphous silicates.^{17–22} However, a lot of information about its production process still remains written in the sample, and nondestructive Raman analysis of the microstructure (by analyzing different positions with microscopic resolution) and nanostructure (through the analysis of the Raman spectra itself) offers a way to retrieve the information, which assists in the identification and sometimes dating of ancient artifacts. On-site analysis is now possible with the use of portable instruments.¹⁸ Many properties of glass depend on its chemical composition, which is a result of the type and ratio of the raw materials used in the batch (mixture of raw materials). All applications in the science, art and technology of glass, glazes and enamels consist of a controlled modification of the three-dimensional Si–O network by replacement of Si^{4+} covalent

*Correspondence to: Philippe Colomban, Laboratoire de Dynamique, Interaction et Réactivité (LADIR), UMR 7075 Centre National de la Recherche Scientifique & Université Pierre et Marie Curie, 2 rue Henri Dunant, 94320 Thiais, France.
E-mail: philippe.colomban@glvt-cnrs.fr

bonded atoms by noncovalent bonded atoms, thereby decreasing the number of Si–O bridges and the connectivity of the network. Consequently, the melting temperature (and the viscosity at a given temperature) decreases. Other physical/chemical properties related to the density and network connectivity (thermal expansion, ion diffusion, reactivity, etc.) are modified accordingly. Direct relationships between the silica content, or more precisely, the ratio of the glass-former (chiefly Si and Al oxides) and the flux (Na, K, Ca, Pb oxides) content, and the properties of glassy silicates have been established for a long time (Seeger's rules and modern developments by Stevels, Huggins, etc. [see, e.g. references in Ref. 12]). Because strong covalent bonded structures have Raman signatures orders of magnitude larger than the ionic ones, the Raman spectrum of a silicate consists, as a first approximation, solely of the signature of the Si–O network (Si–O stretching, bending and librational/collective modes).²¹ Because a SiO₄ tetrahedron is a solid chemical and vibrational entity (molten silicates retain a strong polymeric character), it is well established that the different tetrahedral arrangements – an isolated SiO₄ tetrahedron referred to as Q₀, tetrahedra linked by a common oxygen atom (Si₂O₇ or Q₁), tetrahedra linked by sharing two oxygen atoms (three (Si₃O₉) and *n* tetrahedral cycles: Q₂), by sharing three oxygen atoms (e.g. in some chains, ribbons and layers) and Q₄ (as in pure SiO₂) – have different characteristic Raman signatures.^{18–22}

Our first objective is the classification of representative samples of ancient (Middle Age) and recent (nineteenth century restoration) stained glasses from various cathedrals and churches of France (Amiens, Le Mans, Beauvais, Strasbourg, Rouen and Aube country and others) and glass replicas specially prepared for conservation studies (Sainte-Chapelle, Paris, Saint-Urbain, Troy and Köln Dom, twenty-first century^{23,24}). We will try to establish the Raman signatures of the different compositions used in the preparation of stained glasses – sodium-rich (probably prepared from sodium carbonate or other salts)¹² or potassium-rich (most likely prepared from plant ash) ancient glasses¹² – in order to define a database for on-site identification. One sample of each type was selected for ionic exchange in boiling sulfuric acid. This technique has previously been used to study the corrosion mechanism of sophisticated glass and glass-ceramics used in the aeronautical industry,²⁵ in particular to highlight the diffusion path distribution.^{26,27} Our objective is the quantification of the degree of weathering and a better understanding of the deterioration mechanisms of stained-glass windows.

EXPERIMENTAL

Samples

The objects analyzed are listed in Table 1. A selection of them is shown in Fig. 1. Pieces of stained-glass windows were analyzed as received, without any cleaning or preparation.

Ion exchange

Ion exchange was performed in a round bottomed Pyrex flask using concentrated sulfuric acid, with the volume of acid ~100 times the sample volume.²⁸ We used a sand-filled box with a heater-resistor, capable of reaching 500 °C inside. A water-cooled glass double tube was used to condense the sulfuric acid vapor. Placing the flask in hot sand rapidly heated the samples, which were then exposed to the treatment process for time durations ranging between 5 min and 20 h three times. Samples were washed in water and placed in an ultrasonic bath for a few minutes to remove any soluble sulfates.

Techniques

A multichannel notch-filtered INFINITY spectrograph (Jobin-Yvon–Horiba SAS, Longjumeau, France) equipped with a Peltier-cooled CCD matrix, and two 'XY' spectrographs (Dilor, Lille, France) equipped with a double monochromator filter and a back-illuminated, liquid-nitrogen-cooled, 2000 × 256 pixels CCD detector (Spex, Jobin-Yvon–Horiba Company) were used to record the Raman spectra between 10 (XY instrument)/150 (INFINITY instrument) and 2000 cm⁻¹, using the 457, 488, 514.5, 532, 632.8 and 647.1 nm exciting lines (Ar⁺–Kr⁺, YAG and He–Ne lasers). The power of illumination ranged between 0.5 mW (INFINITY instrument, red samples) and 10 mW (XY instrument, nearly colorless samples) depending on the sample color, instrument and wavelength. Collection of the scattered light in the back scattering geometry was made using a macro setting (volume analyzed ~500 μm³) and through an Olympus confocal microscope (long focus Olympus ×50, ×80 or ×100 objective, total magnification ×500, ×800 or ×1000). A systematic examination was made of the glass surface with the ×50 objective. Ion-exchanged samples were analyzed using the macro setting (XY instrument) and the ×100 objective (Infinity instrument); the size of the confocal hole was decreased to reduce the size of the analyzed volume to a few microns deep. The spectrometer microscope was used to record optical images.

IR spectra were obtained using a 980 Perkin Elmer double-beam spectrometer from samples pressed into CsI pellets. Pieces were broken off, to separate visually grains made of pristine glass from those made of the corroded film, and then each part was separately powdered in an agate mortar.

Compositions

A scanning electron microscope (SEM) (LEO 1530 instrument) was used for the semiquantitative determination of the compositions of ion-exchanged samples. The samples were cut in 3–5 mm plates and covered with a thin Au–Pd film. The EDX analysis (EGG instrument, Bruker software) was then performed in the range between 1 and 15 keV. The analysis could be performed on an area several μm in diameter.

A series of samples from the bulk of the material were embedded in a polyester SODEMI H59 resin, polished and observed using a Jeol JSM 5600 low-vacuum SEM. Further analyses of the microstructure were made using a Jeol JSM 840 instrument to determine the mean glass composition (Link ISIS system, ZAF quantitative correction method). Compositions of glass replicas made in the twenty-first century were taken from Ref. 23. These K–lime silica glasses, replicating the thirteenth- and fourteenth-century glass compositions of three ancient monuments, were exposed *in situ* during a one-year in-field experimentation by VIDRIO, the European program for stained-glass window conservation.²⁴

Peak fitting and data processing

In undertaking a curve-fitting of the Raman spectra, a linear baseline was first subtracted using the LabSpec software as previously discussed.^{21,22,29} We selected a 4-segment baseline: ~150–700, 700–890, 890–1300 and 1300–1700 cm⁻¹ for a reproducible separation of the different components of the Raman signatures. The same spectral windows were used for the extraction of the components using the Origin

peak-fitting software module (Microcal Software, Inc.). The integral area, the bandwidth and the center of gravity were calculated for each component using the Q_n model.^{21,22} This model allows for a comparison of the glassy silicate nanostructure over a large composition range. A Gaussian shape was chosen for all Raman lines assigned to glassy silicates because of the amorphous state of the examined materials. A Lorentzian shape was used for the narrow components.

Silicate structures consist of more or less connected (polymerized) SiO₄ tetrahedra. Because the SiO₄ tetrahedron is a very well defined vibrational and structural entity, its different configurations have specific vibrational fingerprints. The different spectral components provide information on the connectivity of the SiO₄ polymeric units and therefore on the glass composition, nanostructure and processing temperature. A clear differentiation is possible through evaluation of the relative intensities of the components of the Si–O stretching and bending modes at *ca* 1000 and 500 cm⁻¹, respectively and from I_P, the polymerization index, defined as I_P = A₅₀₀/A₁₀₀₀, A being the area under the Raman band. From the literature (Refs 17–23 and references therein), the

Table 1. Samples studied in this work. Samples in italics have been selected for ion-exchange treatment

Origin	Date (century)	Color	Label	Type
Amiens cathedral	19th	Green	AM19vert	1
<i>Amiens cathedral</i>	<i>19th</i>	<i>Greenish</i>	<i>AM19verdâtre</i>	1
Amiens cathedral	19th	Purple	AM19pourpre	1
Aube church	15–16th	Pale purple	AU15	1
<i>Amiens cathedral</i>	<i>19th</i>	<i>Amber-yellow</i>	<i>AM19jaune</i>	2
Amiens cathedral	13th(?)	Yellow + grisaille (glass paint)	AM0	3
Amiens cathedral	13th	Pale green	AM1	3
Amiens cathedral	13th	Blue	AM3	3
Amiens cathedral	13th	Blue + 'grisaille' (glass paint)	AM5	3
Amiens cathedral	13th	Blue	AM14	3
Aube church	15–16th	Colorless glass with a red flashed layer	AU9	3
Amiens cathedral	13–14th	Colorless glass with a red flashed layer	AM13	3
Amiens cathedral	13–14th	Colorless glass with a red flashed layer	AM22	3
<i>Amiens cathedral</i>	<i>19th</i>	<i>Dark blue</i>	<i>AM19bleu</i>	3
Le Mans	13–15th	Pale blue	LM3	3
Le Mans	13th	Blue	LM8	3
Köln	21st	Pale brown (Vidrio 7d)	C1	3
Köln	21st	Green (Vidrio 12d)	C2	3
Sainte-Chapelle	21st	Blue (Vidrio)	SC21bleu	3
Sainte-Chapelle	21st	Violet (Vidrio)	SC21mauve	3
Troyes Basilica	21st	Pale yellow (Vidrio)	TR21jaune	3
Aube church	15–16th	Pale green	AU8	3bis
Aube church	15–16th	Blue	AU16bleu	3bis
Beauvais cathedral	17th	Blue	B1	3bis
Aube	15–16th	Lavender blue	AU2	3bis
Strasbourg	14–15th	Colorless glass with yellow layer	S1	3bis
Rouen	15th	Yellow-brown	R1	3bis

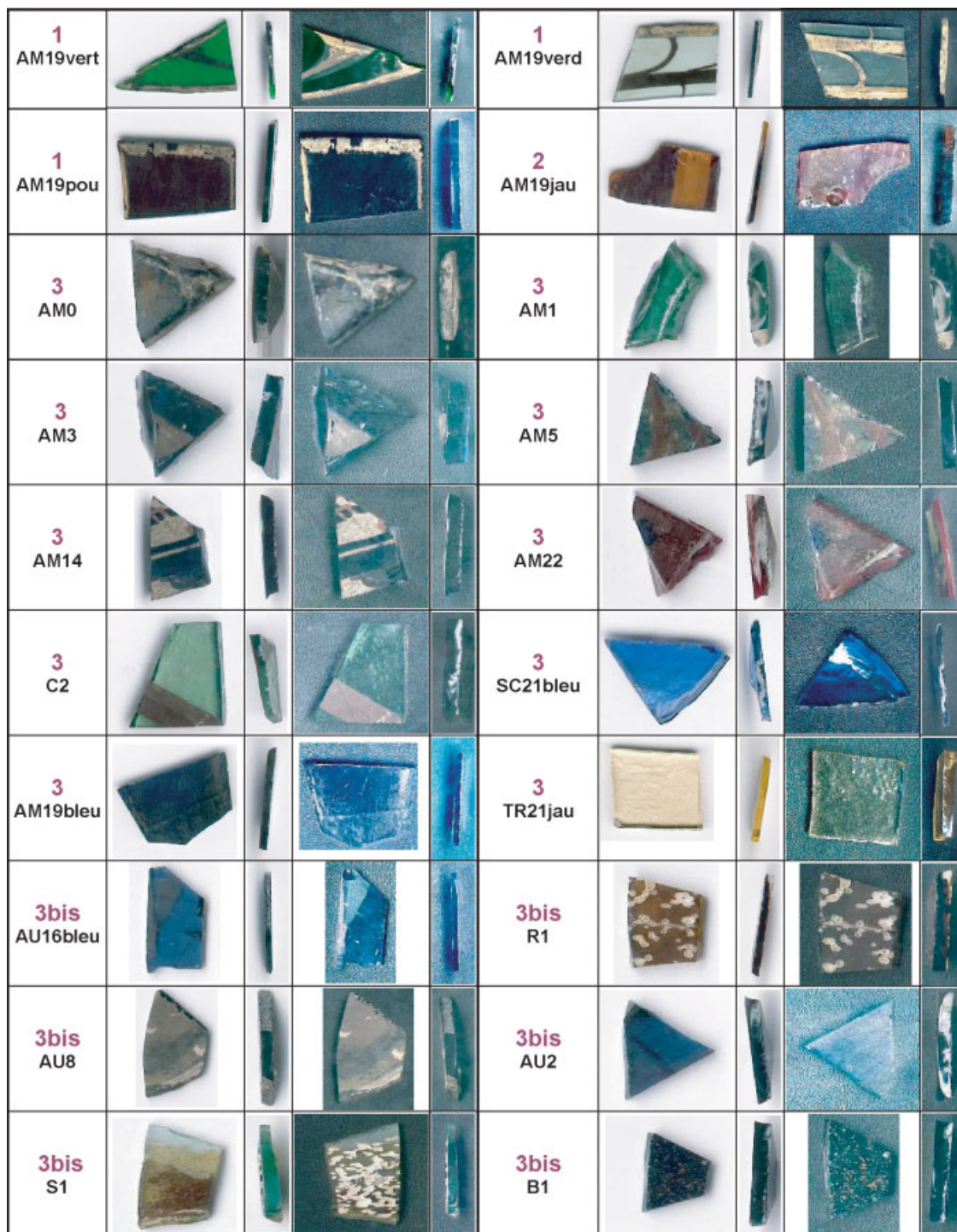


Figure 1. Examples of glass pieces studied. Note the corrosion dots of some glasses. Samples have been scanned on their flat surface and cut sections, as well on white and black paper, to highlight the grisaille and the corrosion dots.

different spectral components of the stretching envelope were assigned to specific silica vibrations. The following assumptions were made: (1) For the Si–O stretching range extending from 700 to 1300 cm^{-1} (see previous work), we postulated five components namely Q_0 , Q_1 , Q_2 , Q_3 and

Q_4 according to the number of oxygen atoms bonded per tetrahedron. (2) We also postulated five bands with similar bandwidths for Si–O bending components. (3) One or two narrow bands were added, if necessary, to take crystalline phases into account.

RESULTS

Classification

Figure 2 shows representative Raman spectra recorded on the samples listed in Table 1 (photographs in Fig. 1). In this preliminary work, we identified three types of Raman signatures, referred to as Type 1, 2 and 3 (see Fig. 3 for selected spectra with decomposition of the Q_n components and Table 2 for the corresponding Q_n and I_p values). The signatures of red flashed glass and of silver-yellow painted glass will not be considered here, because of the unique character of the Raman signature of materials with a metal nanoprecipitate distribution.³⁰

Type 3 glass corresponds to group 6 ('K₂O + CaO' glass) according to our previous classification of glassy silicates^{17,21,29} while Type 1 and Type 2 glasses belong to group 3 ('Na₂O + K₂O + CaO' glass), a group that encompasses most of the ancient glasses, e.g. the Phoenician–Roman glasses.³¹ Characteristic component wavenumbers and peak areas are given in Table 2 after subtraction of a linear segment baseline (see Refs 22 and 29 for a discussion of the

procedure). Type 3 signature consists of a strong Si–O bending peak at 590–620 cm⁻¹ and a strong broad Si–O stretching peak at ~1080–1090 cm⁻¹, with a narrow peak at ~950 cm⁻¹.

Type 2 signature is rare (only one occurrence, the AM19jaune glass); the intensity of the 950 cm⁻¹ peak is greatly diminished and the main Si–O stretching mode peaks at ~1100 cm⁻¹. Additionally, a rather strong peak is observed at ~460 cm⁻¹. Type 1 signature is recognizable from the 950–995 cm⁻¹ doublet and the rather large area of the 450 cm⁻¹ band. An additional Type 4 signature is observed in the red copper-doped layer of the flashed glass, with a characteristic strong ~500 cm⁻¹ component and 625 cm⁻¹ shoulder³⁰ and will not be discussed in this paper.

A group of glass that we refer to as 3bis has a signature that is similar to the Type 3 signature, but with the following obvious differences: the intensity of the 450 cm⁻¹ broad peak is larger and many components are observed. Note that all these glasses exhibit a number of corrosion dots (Fig. 1).

Comparison with the EDS analysis shows that Type 1 glass is a Ca-rich, Na-containing silicate, Type 2 glass is

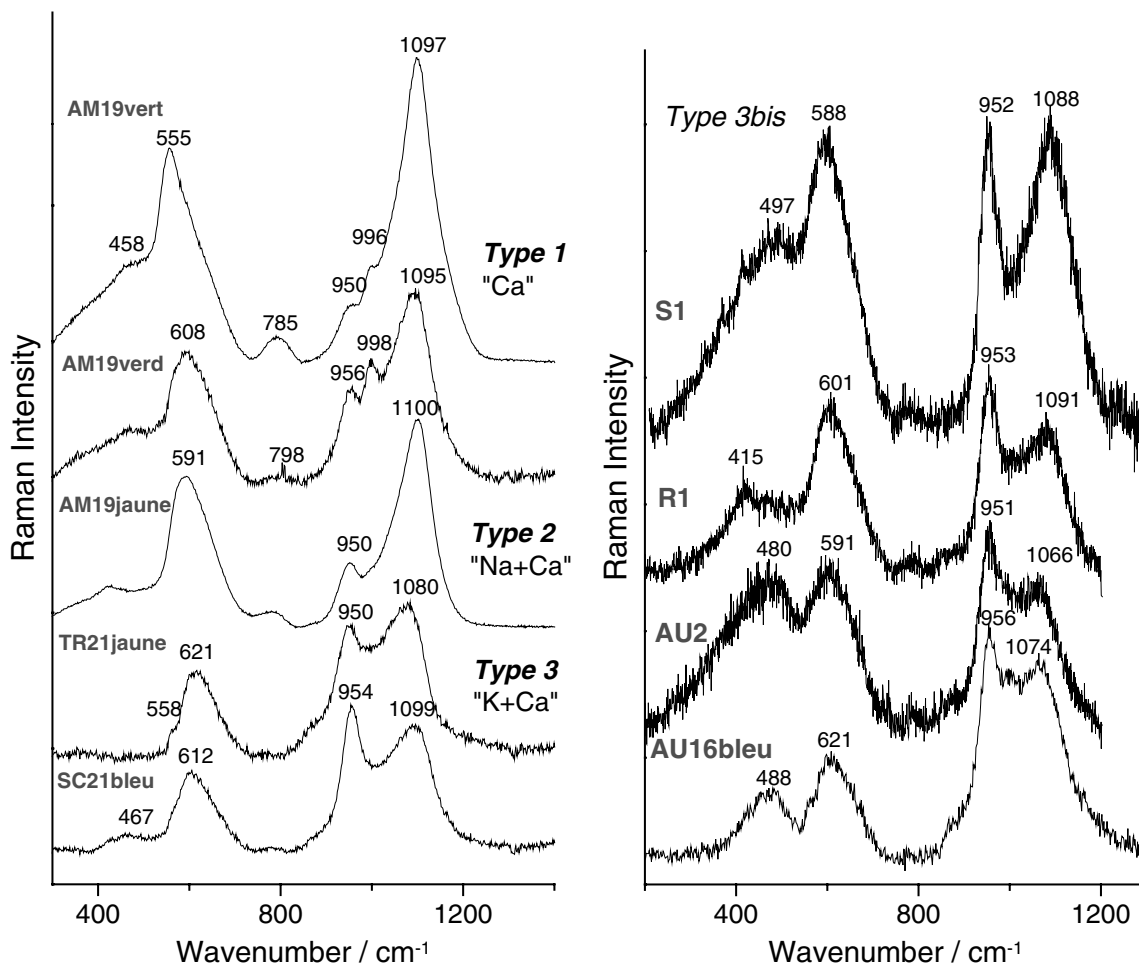


Figure 2. Representative Raman spectra selected from among those listed in Table 1. Spectra have been recorded at the sample surface (analyzed depth >50 μm or more).

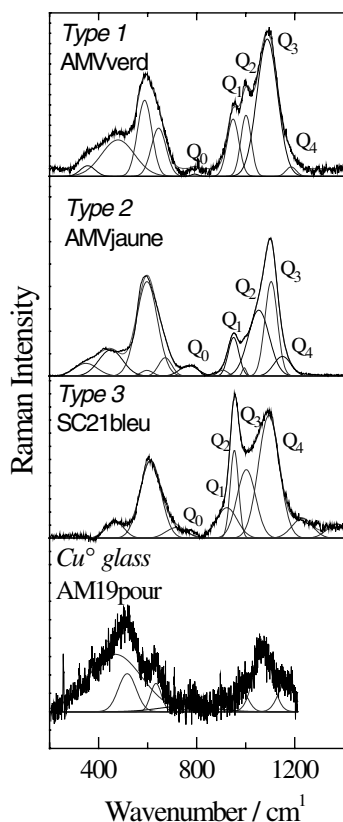


Figure 3. Representative Raman signatures of the three types of stained glasses. Baselines have been subtracted following the 4-segment procedure, which eliminates the Boson peak. The signature of red-metal-particle containing sample (red flashed glass) is also shown. Wavenumbers and peak area components are given in Table 2.

a Na-rich, Ca-based silicate and Type 3 glass is a K–Ca silicate (Fig. 4). Table 3 compares the mean compositions of a selection of glass of each group (ancient, modern and glass replicas). Obviously, the large structural differences evidenced from the Raman spectra are less clear from a simple comparison of the oxide content. The CaO/Na₂O and CaO/K₂O ratio must be considered.

Ion exchange and reactivity of the different glasses

Figure 5 compares the sample sections obtained by breaking the representative glass pieces after 20 h of thermal treatment in boiling concentrated sulfuric acid. The pristine state and initial color still remains in the core of the bulk sample. A more-or-less thick white or pale colored film is formed all over the surface. The mechanical strength of the film is still high, which is an indication that the glass network connectivity has been preserved. However, the loss of transparency indicates that microcracks, pores and/or second phases have formed. The thickness of the film was measured and plotted as a function of time and square root of time in Fig. 6. Optical observations on representative sections and surfaces are given in Fig. 7 and the compositional change is illustrated with the EDS spectra in Fig. 4.

The idea in using sulfuric acid attack is to accelerate the exchange of mobile cations with H₃O⁺ ions, which was confirmed by the presence of the characteristic bending mode at 1750 cm⁻¹ in the IR spectra of the glass^{28–32} (Fig. 8 and Table 4). More complex protonic entities are however possible.^{28,32,33} It is therefore easy to analyze the glass modification with a variety of techniques including vibrational spectroscopy, which is a very powerful technique for the study of amorphous silicates.

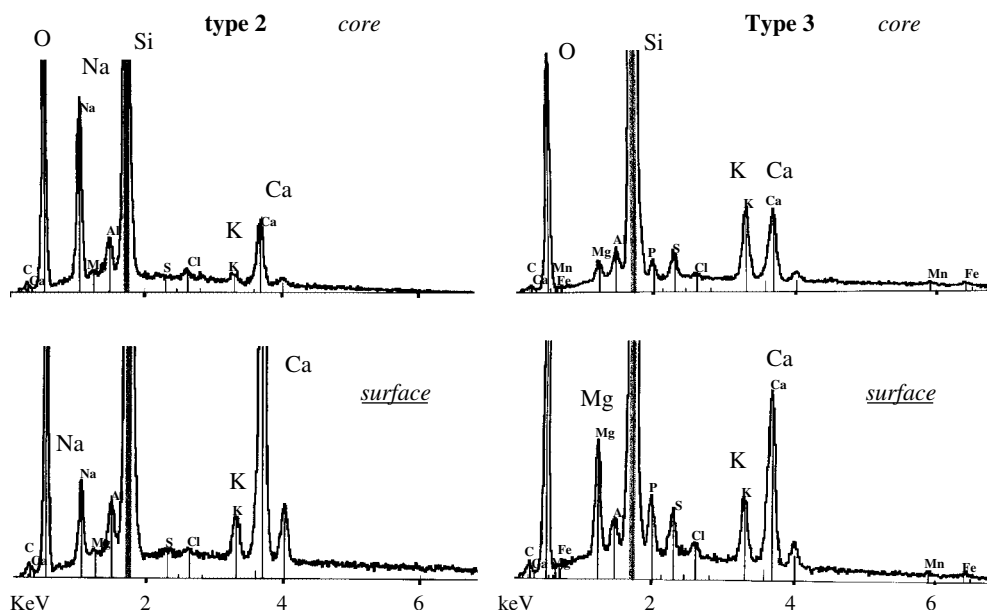


Figure 4. Comparison of EDS spectra recorded on pristine glass core (top) and surface film section (bottom) after 20 h treatment in sulfuric acid. Samples were broken just before the examination.

Table 2. Raman component wavenumber (Q_n) and polymerization index (I_p) of representative samples (Types 1, 2 and 3 glasses). Spectra have been recorded at the sample surface (analyzed depth $>50 \mu\text{m}$)

Items	I_p	Q_0 (cm^{-1})	Q_1 (cm^{-1})	Q_2 (cm^{-1})	Q_3 (cm^{-1})	Q_4 (cm^{-1})
Type1	–	–	–	–	–	–
AM19vert	0.99	792	948	1047	1100	1149
AM19pourpre	0.72	792	940	1002	1096	1185
AM19verdatre	0.75	800	940	1002	1090	1164
AU15	1.2	786	875	995	1080	1154
Mean value	0.92	792.50	925.75	1011.50	1091.50	1163.00
Δ	0.23	5.74	34.04	23.90	8.70	15.94
Type2	–	–	–	–	–	–
AMvjaune1	0.94	769	950	1053	1104	1150
Type3	–	–	–	–	–	–
AM0	1.5	782	906	997	1086	1186
AM1	0.9	780	875	988	1080	1159
AM3	0.8	782	858	1011	1083	1151
AM5	1	779	873	1014	1081	1133
AM14	0.8	787	868	1008	1080	1158
AU9	1	778	847	988	1082	1190
AM13	0.8	793	869	983	1060	1169
AM22	1.3	779	875	1004	1073	1116
AM19bleu	0.73	774	926	1003	1093	1178
LM3	0.6	776	874	1007	1077	1139
LM8	0.7	773	875	995	1067	1114
C1	0.9	795	868	1013	1076	1160
C2	0.8	780	871	995	1060	1120
SC21bleu	0.67	776	923	1001	1088	1246
SC21mauve	0.66	787	870	967	1086	1241
TR21jaune	0.77	776	884	1009	1084	1170
Mean value	0.87	781.06	878.88	998.94	1078.50	1164.38
Δ	0.24	6.43	21.54	12.68	9.46	38.85
Type3bis	–	–	–	–	–	–
AU8v1	1.2	784	880	991	1069	1144
AU16bleu	0.96	776	884	1001	1080	1164
B1v1	0.9	788	871	1006	1077	1153
AU2v1	1.4	788	866	999	1066	1136
R1v1	1	784	860	1016	1091	1160
S1v1	1.2	781	849	1014	1088	1152
Mean value	1.11	783.50	868.33	1004.50	1078.50	1151.50
Δ	0.19	4.55	12.94	9.48	9.97	10.27

Type 1 glass is almost insensitive to the action of sulfuric acid. The thickness of the layer modified after 20 h in sulfuric acid is only a few microns ($\sim 0.05 \mu\text{m/h}$). On the other hand, the film layer reaches $\sim 350 \mu\text{m}$ ($\sim 15 \mu\text{m/h}$) and $\sim 600 \mu\text{m}$ ($\sim 30 \mu\text{m/h}$) for Type 2 and Type 3 glasses after the same duration of chemical attack (Fig. 6). Plots as a function of the square root of time show a two-step process, first a very slow one and then a fast one with the same activation energy for Type 2 and 3 glasses (straight lines are parallel). EDS analyses show strong K, Na and moderate Ca–Al loss.

The examination of the microstructure (Fig. 7) showed different phenomena. We will discuss only the results obtained on Type 3 samples after 5 min and 20 h in sulfuric acid, which are representative of the main features.

After 5 min of boiling in sulfuric acid we observe a modification of the surface: a number of cracks are formed in the first $10 \mu\text{m}$ of the outer surface, and then a regular network of microcracks perpendicular to the surface extend to hundreds of microns in depth. This type of crack formation is consistent with glass shrinkage, as observed for many

Table 3. Examples of representative compositions of Type 1, 2 and 3 glasses

Oxide/%	Type 1	Type 2	Type 3 (K–Ca silicate)	
	(Ca silicate)	(Na–Ca silicate)	Ancient	Replica
SiO ₂	60–70	63	50	53
Al ₂ O ₃	2–3	2	2.5	2
Na ₂ O	8–14	18	1–3	1
K ₂ O	0.5–1.5	1.5	18.5	18
CaO	16–18	15	14.5	16
MgO	2.5	0.2	4–6	5
P ₂ O ₅	0.2	<0.05	3.5–4	4
Fe ₂ O ₃	0.5	0.2	1	0.5
MnO	0.3	<0.1	1	1
PbO	0.6	0	0	0
Others	<1	<1	<1	<1
CaO/Na ₂ O	1–2	0.8	>6	16
CaO/K ₂ O	>10	10	~0.8	~0.9

Table 4. Assignment of IR bands of representative samples (Types 2 and 3 glasses) before and after acid sulfuric treatment

Type 3 glass (cm ⁻¹)	H ₂ SO ₄ treated ^b	Type 2 glass (cm ⁻¹)	H ₂ SO ₄ treated ^b	Assignment
pristine ^a	H ₂ SO ₄ treated ^b	Pristine ^a	H ₂ SO ₄ treated ^b	–
285 w	255 w	255 vw	260 vw	R' SiO ₄
		410 sh		
460 s	465 s	468 s	460 s	δ Si–O
500 sh		510 sh		
605 w	600 w	610 sh	620 w	
670 vw				
775 m	800 m	770 m	795 m	ν Si–O–Si
950 sh		950 s		
1030 vs	1100 vs	1050 vs	1080 vs	ν Si–O
1180 sh	1220 sh		1250 sh	
1600 w		1600 w		
	1635 w		1660 w	δH ₂ O
	1720 w	1720 vw	1740 w	δH ₃ O ⁺

s – strong; vs – very strong; m – medium; sh – sharp; w – weak; vw – very weak.

^a Powdered sample core.

^b Powdered surface film.

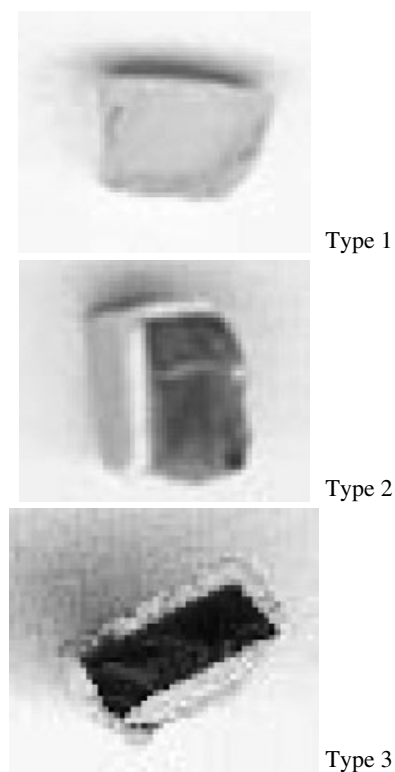
(earth) alkali silicates,^{25,26} owing to the loss of K ions (Fig. 4). The rather regular distance between the cracks perpendicular to the surface arises from a combination of the amount of shrinkage due to ion exchange and the mechanical strength of the glass. Note that the distance between cracks is about

10 times smaller in the outer surface. This indicates that the composition of the external surface is different from the bulk and/or that the deterioration mechanism was different, according to the two-step behavior observed on the thickness plotted as a function of the square root of time.

After 20 h in sulfuric acid, six different layers are observed (Fig. 7(c)), from the top surface to the pristine glass core:

- a surface layer, in which K⁺ (and/or Na⁺) ions have been exchanged by protonic species; this layer is not optically clear anymore. Note that the interface between the opaque surface layer and the substrate is not flat, indicating a large variation in glass reactivity.
- an optically clear layer, with cracks perpendicular to the surface (as observed after the 5-min treatment (Fig. 7(b)), in which fractal animal figures are visible.
- a dark, nearly flat interface is observed, superimposed on a layer with some corrosion pathways and cracks.
- finally, at the interface with the pristine glass, the complex round figures indicate localized modifications that could be linked to heterogeneity in the composition of the pristine glass.

Examination of the glass surface from the top (Fig. 7(d)) shows a rather regular crack network made of circular cracks linked by nearly linear cracks. Such regular circular distribution can be correlated to an ordered heterogeneity.

**Figure 5.** Sample sections after 20 h of thermal treatment in sulfuric acid for the different types of glasses.

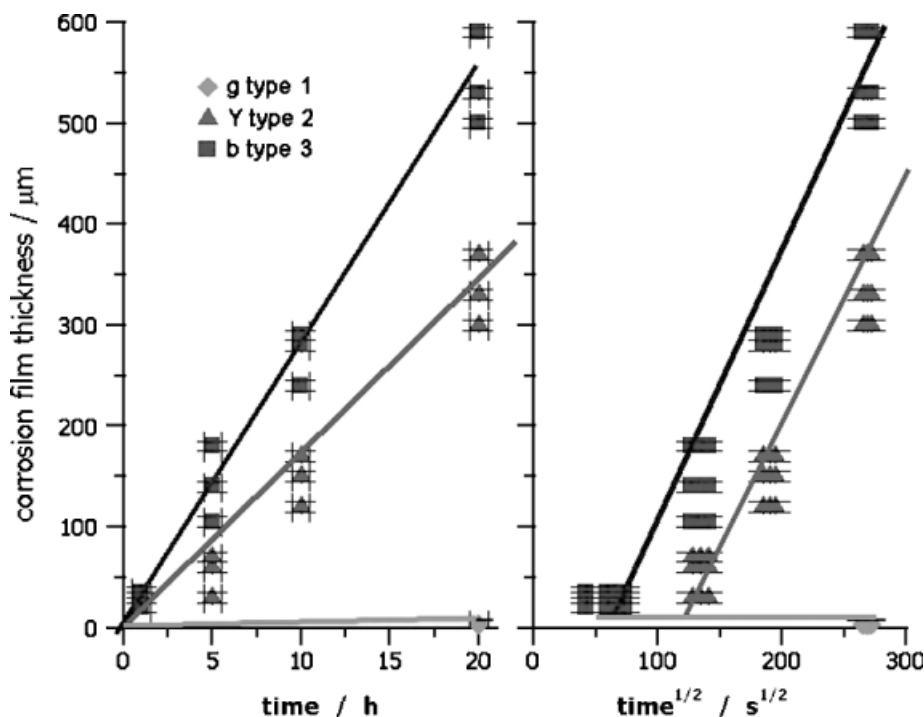


Figure 6. Corrosion film thickness as a function of sample type plotted against time and square root of time.

IR spectra were obtained of Type 2 and Type 3 powdered cores and films (Fig. 8). Nanostructural changes are evident with the shift in the maxima of certain peaks (e.g. the Si–O–Si mode shifts from 770/775 to 795/800 cm⁻¹ for Type 2 and Type 3 glasses) and the disappearance of many shoulders (e.g. the 950 cm⁻¹ on the main Si–O asymmetric stretching mode). Additionally, a weak peak at ~1740 cm⁻¹ is observed in ion-exchanged materials, owing to the substitution of alkali ions by oxonium^{26,28,32} and the compositional changes illustrated in Fig. 4 (see the strong decreases of the Na and K (and Al) EDS signatures in the films).

In this preliminary investigation, we limited our Raman analyses to the upper surface. The analysis of the interface between the homogeneous film and the sound pristine glass will be presented in a further paper. Representative Raman spectra are given in Fig. 9 for samples after different periods of sulfuric acid attack. We observe the following:

- a shift of the main Si–O stretching peak from ~1090 (Type 1 and 2 glass) or 1075 cm⁻¹ (Type 3 glass) to 1080 (Type 1), 1070 (Type 2) and 1060 (Type 3) cm⁻¹.
- a decrease in the intensity of the broad Si–O bending peak (~570 cm⁻¹) and of the ~950 cm⁻¹ narrow component.
- a decrease in the Boson peak.

All these changes indicate a modification of the silicate network according to shrinkage, and the loss of Na⁺, K⁺ and to a lesser extent of Al³⁺ and Ca²⁺ ions.

DISCUSSION

Important results were obtained from this preliminary study. First, ion-exchange substitution of K⁺ and Na⁺ ions induced clear modifications of the Raman signature, and strong discrepancies are observed between the different types of glass. Obviously the 3bis type glass corresponds to weathered silicates in the analyzed surface volume, about 10 to 50 µm deep for our conditions. Visual observation of these samples (Fig. 1) shows many white pits at the glass surface made of complex carbonates/sulfates as secondary alteration products. Raman data were always collected in areas outside the pits, in the apparently 'safe' glass. Therefore our objective of establishing Raman scattering as an on-site measurement technique of the degree of corrosion appears to be a reasonable one.

Cut glass cross sections exposed different layers with both homogeneous and heterogeneous characters. In the future, we will try to examine the Raman signature of the different zones, to confirm whether this behavior is related to compositional or structural heterogeneity of the original glass. Note that such complex figures of corrosion have been reported for a long time without a clear explanation.^{6,9} It is important to note that the microcrack network observed at the sample surface (Fig. 7) is less 'fractal' than those observed for lithium aluminosilicate glasses in which conducting pathways are tubular.^{26,27} In particular, we observe from place to place circular cracks that support compositional and structural heterogeneity (for instance, Na/K/Ca-rich and Na/K/Ca-poor, silica-rich regions, as sketched in Fig. 10).

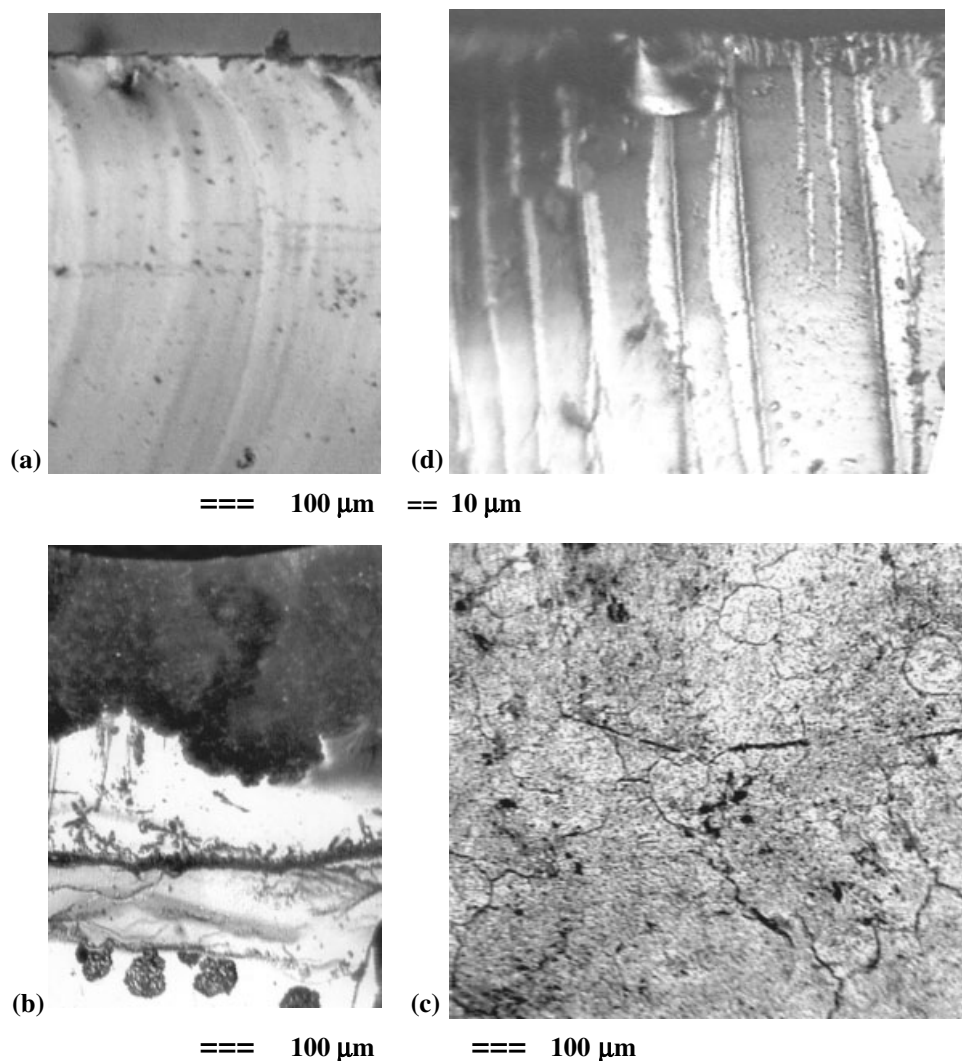


Figure 7. Representative microstructures of 20-h-treated Type 1 (a) and Type 3 (b) sample sections; 20-h-treated Type 3 surface (c); 5-min-treated Type 3 sample section (d).

Local composition heterogeneity has been already postulated in the Modified Random Network.³⁴

The polymerization index of the pristine glasses are rather similar (~ 0.9 , Table 2). This is not surprising because whatever the composition of raw materials, glass manufacturers endeavored to obtain a material that could be prepared in the same range of temperatures (our previous work has unambiguously established the strong correlation between the polymerization index and the processing temperature of glassy silicates^{21,22}). Note that the scattering of the value is close to 0.2 for both Type 1 and Type 2 groups. The polymerization index measured for Na/K-depleted glasses is higher (~ 1.1), according to the loss of alkali ions and of some less connected $(\text{SiO}_4)_n$ entities, equivalent to an increase of the silica content in the depleted film. These conclusions are correlated with the EDS analysis and with the increase of the $\sim 450 \text{ cm}^{-1}$ Si–O bending peak. The disappearance of the narrow peak at $\sim 950 \text{ cm}^{-1}$, assigned to potassium/calcium

silicate nanocrystals (the correlation between potassium content and the intensity of this peak was previously noted³⁵) confirms that less connected entities are unstable in acidic environments and that they are not only related to the potassium content but also to the calcium content. Note that the strong and narrow 950 cm^{-1} peak position is very similar to that of wollastonite, a calcium nesosilicate that precipitates very easily in Ca-saturated glasses and glazes.¹⁷ The relatively small FWHM of this peak was not expected for a usual Q_1 or Q_2 component of a glassy silicate and fits better as a signature of some nanocrystals dispersed in the glass. However, the 950 cm^{-1} peak is stronger than the $\sim 1060 \text{ cm}^{-1}$ one for Ca-rich glasses (for instance, Köln C2 glass: $\text{SiO}_2 \sim 46 \text{ wt}\%$, $\text{K}_2\text{O} \sim 11\%$ and $\text{CaO} \sim 30\%$). Obviously the plot of the 950 cm^{-1} intensity *vs* the wavenumber of the ν Si–O stretching component at 1060 to 1090 cm^{-1} as a function of the K and Ca content would be very useful to the understanding of the relationship between the Raman

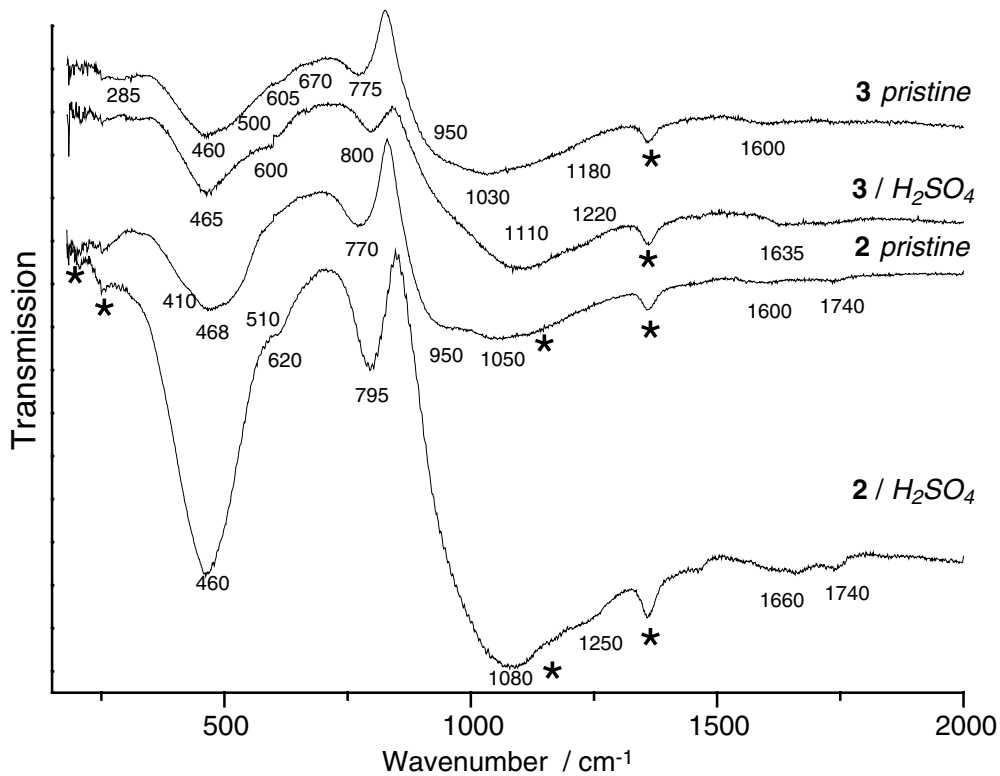


Figure 8. Representative IR spectra showing the transformation of the pristine glass in the ion-exchanged silicate network for Type 3 (K–Ca) and Type 2 (Na–Ca) glass; * indicates impurities of the CsI matrix.

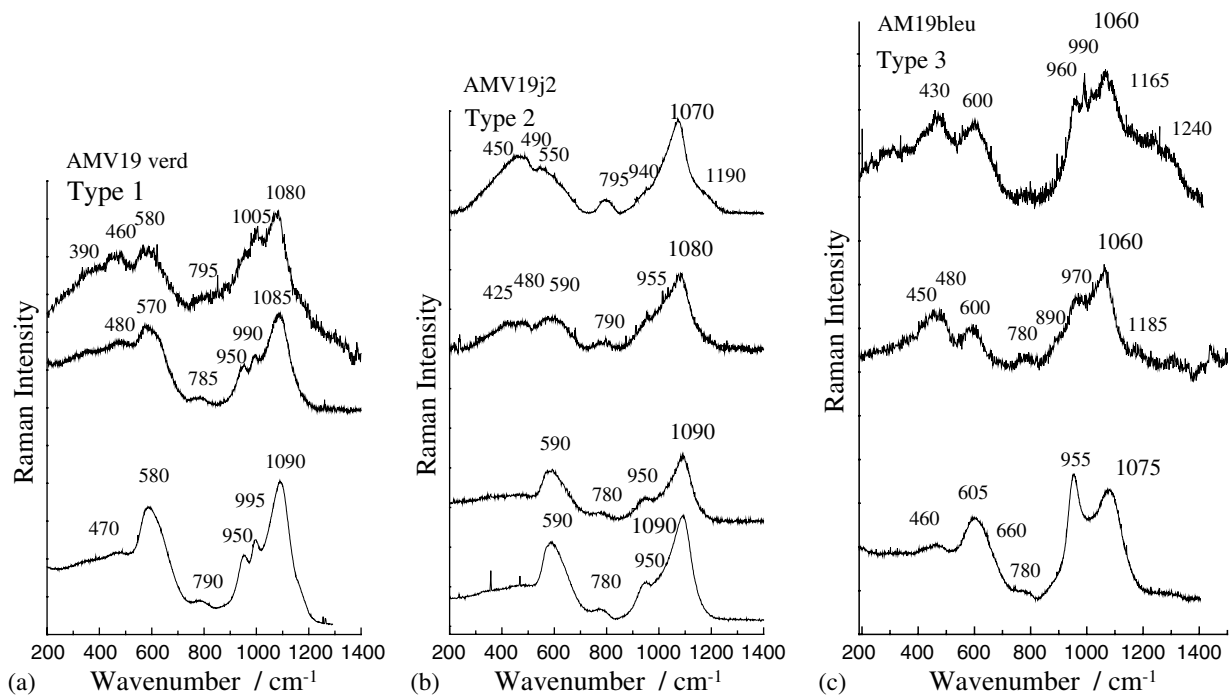


Figure 9. Representative Raman spectra showing the transformation of the pristine glass in the ion-exchanged silicate network; bottom, macro spectra: pristine glass, no base line was subtracted; other spectra: recorded at the sample surface after (10- and 20-h treatment in sulfuric acid, using macro setting (analyzed depth >100 μm); top spectra have been recorded under a microscope to highlight the structure of the outer surface layer (analyzed surface from ~10 μm for Type 3 sample to ~2 μm for Type 1 sample).

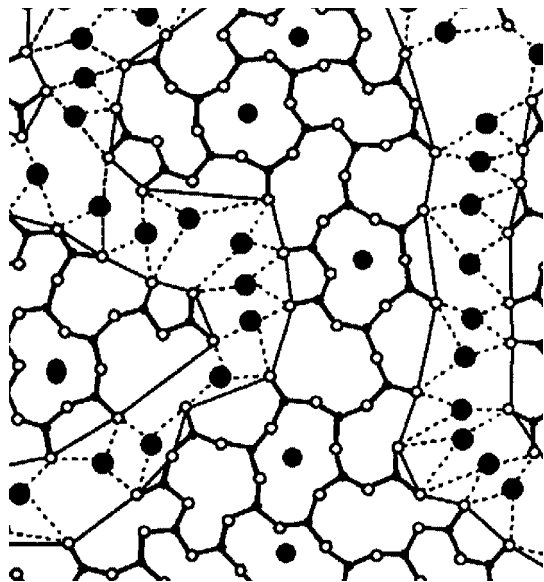


Figure 10. Sketch of the silicate network according to the modified random network, after Ref. 34, showing the alkali ion heterogeneity.

signature and glass composition. Figure 11 shows the plot of the area of the $\sim 590\text{ cm}^{-1}$ peak (normalized with respect to the other components of the δ Si–O envelope) as a function of the 950 cm^{-1} one (normalized with respect to the other components of the ν Si–O envelope). The highest values, close to 0.9, are measured for Type 3 glasses, although much lower values are obtained for Type 3bis weathered glasses. Simultaneously, the wavenumber of the ν Si–O maxima shifts downwards. Substitution of alkali ions by oxonium and the associated loss of less polymerized $(\text{SiO}_4)_n$ entities (also seen by the accompanied loss of Al^{3+} ion) not only modify the geometry of the Si–O–Si– network but also involve changes in oxygen polarization and hence in the Raman band intensity, a poorly documented subject.

CONCLUSIONS

The study of a representative series of stained glass dating from the thirteenth to seventeenth, nineteenth (modern) and twenty-first centuries (glass replicas) enabled us for a preliminary classification the glasses into four types, Type 1 (rare Ca-rich silicate), Type 2 (extremely rare, Na-rich, Ca-silicate), Type 3 (main group, K–Ca silicate) and a variant Type 3 referred to as 3bis. Ion exchange of the alkali cation took place in boiling sulfuric acid to mimic the first step in the glass deterioration, and the subsequent structural and compositional changes have been analyzed with IR and Raman spectroscopy, optical microscopy and EDS. Measurements of the film thickness show a great discrepancy between the ion-exchange rates of K–Ca (Type 3: $60\text{ }\mu\text{m/h}$) and Na–K (Type 2: $15\text{ }\mu\text{m/h}$) silicates and that of Type 1 silicate ($0.05\text{ }\mu\text{m/h}$), a very stable glass. IR and Raman

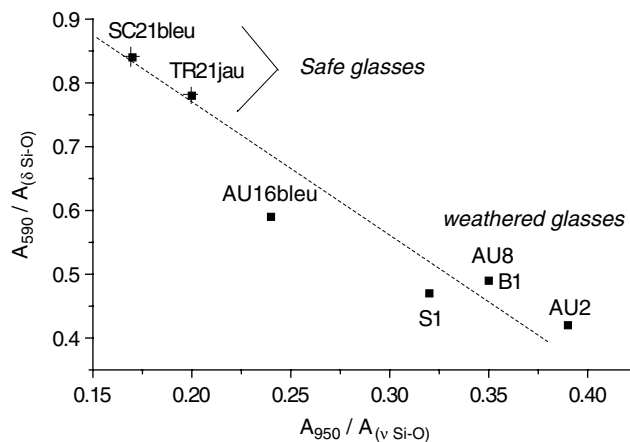


Figure 11. Plot of the relationship between the peak area of the ca 590 cm^{-1} band (normalized against the δ Si–O massif) and the 950 cm^{-1} band (normalized against the ν Si–O massif).

spectra provided evidence of nanostructural modifications, chiefly the downward (Raman) and upward (IR) shift of the main Si–O stretching peak and the decrease in intensity of the Boson peak, as well as the Raman 580 cm^{-1} Si–O bending peak. The intensity of the narrow $\sim 950\text{ cm}^{-1}$ Raman peak, assigned to (earth)alkali nano crystallites in the glassy network, is correlated to the K/Na loss and glass deterioration. Consequently, Type 3bis samples are in fact glass, the surface of which is depleted of K/Na ions, and the ratio of both the $\sim 460/590$ and $950/1090\text{ cm}^{-1}$ peak areas appears to be a good parameter to quantify the degree of deterioration of stained glasses (Fig. 11). Optical micrographs show the macroscopic heterogeneity of the nanostructure and composition of the ancient glass, which supports similar heterogeneity on a smaller scale (Fig. 10), with preferential ‘regions’ for ion diffusion. In a future work we hope to obtain Raman images of these regions, which would link the optical observations of heterogeneous nanostructures to their chemical composition. These innovative results, which already demonstrate the potential of Raman scattering for *in situ* measurement of the degree of deterioration of ancient stained glass, merit a long-term research project.

Acknowledgements

The authors thank Mrs Isabelle Pallot-Frossard, director of LRMH, for her help and support. Special thanks are due to Drs Léo Mazerolles and Marie-France Trichet (CECM, CNRS, Vitry) for some EDS measurements and to the C2RMF (Musée du Louvre, Paris) for the use of its MEB facilities. Mr François Romain and Gérard Sagon are acknowledged for their technical help and Mrs Linda Prinsloo (University of Pretoria) for her critical reading of the manuscript.

REFERENCES

- Clark DE, (Ed). *Corrosion of Glass*, Books for Industry and the Glass Industry. New York, 1979.
- Newton RG. The deterioration and conservation of painted glass, a critical bibliography. *Corpus Vitrearum Medii Aevi Great Britain*

- Occasional Paper II*. British Academy, Oxford University Press: Oxford, 1982.
3. Perez y Jorba M, Dallas JP. *News Letters du Comité Technique du Corpus Vitrearum* 1984; **37–38**: 8.
 4. Perez y Jorba M, Dallas JP, Collongues R, Bahezre C, Martin JC. *Rivista della Stazione Sperimentale del Vetro* 1984; **5**: 121.
 5. Gillies KJS, Cox GA. *Glastechnische Berichte* 1988; **61**: 75.
 6. Cox GA, Ford BA. *J. Mater. Sci.* 1989; **24**: 3146.
 7. Newton R, Davison S. *Conservation of Glass*. Butterworth: London, 1989.
 8. Perez y Jorba M, Mazerolles L, Michel D, Rommeluère M, Bahezre C. *Compte-rendu du 1^{er} Colloque du Programme Franco-Allemand de recherche pour la Conservation des Monuments Historiques*, 1993; 213.
 9. Cox GA, Ford BA. *J. Mater. Sci.* 1993; **28**: 5637.
 10. Bunker BC. *J. Non-Cryst. Solids* 1994; **179**: 300.
 11. Bunker BC, Arnold GW, Beauchamp EK. *J. Non-Cryst. Solids* 1983; **58**: 295.
 12. Pollard AM, Heron C. *Archaeological Chemistry*. RSC Paperbacks: Cambridge, 1996; 149, Chapt. 5.
 13. Verità M. *Glass, its Nature, Properties and Deterioration Mechanisms, in Sciences and Technologies of the Materials and of the Environment for the Protection of Stained-Glass and Stone Monuments*, Créteil, 1998; 29.
 14. Libourel G, Sterpenich J, Barbey P, Chaussidon M. Caractérisation microstructurale, minéralogique et chimique de l'altération des vitraux. In *Le matériau Vitreux: Verre et Vitraux*, Lefèvre R-A, Pallot-Frossard I (eds). Centro Universitario Europeo per i Beni Culturali: Ravello, 1998; 75.
 15. Römich H. Laboratory experiments to stimulate corrosion on stained glass window. In *The Conservation of Glass and Ceramics*, Tennent NH (ed). James: London, 1999; 57.
 16. Robinet L, Eremin K, Fearn S, Pulham C, Hall C. *Mater. Res. Soc. Symp. Proc.* 2005; **852E**: OO8.8.1.
 17. Colomban Ph. Glasses, glazes and ceramics – recognition of the ancient technology from the Raman spectra. In *Raman Spectroscopy in Archaeology and Art History*, Edwards HGM, Chalmers JM (eds). Royal Society of Chemistry: London, 2005; 192, Chapt. 13.
 18. Colomban Ph. *Mater. Res. Soc. Symp. Proc.* 2005; **852E**: OO8.3.1.
 19. Mysen BO, Virgo D, Scarfe C. *Am. Mineral.* 1980; **65**: 690.
 20. Seifert F, Mysen BO, Virgo D. *Am. Mineral.* 1982; **67**: 696.
 21. Colomban Ph. *J. Non-Cryst. Solids* 2003; **322**: 180.
 22. Colomban Ph, Paulsen O. *J. Am. Ceram. Soc.* 2005; **88**: 390.
 23. Geotti-Bianchini F, Nicola C, Preo M, Vallotto M, Verità M. *Rivista della Stazione Sperimentale del Vetro* 2005; **35-3**: 49.
 24. Etcheverry MP, Trocellier P, Djanarthany S, Beck L, Magasouba B. *Rivista della Stazione Sperimentale del Vetro* 2005; **35-3**: 63.
 25. Colomban Ph. *Mater. Sci. Forum* 1997; **251/254**: (Pt. 2): 835.
 26. Scanu T, Gugliemi J, Colomban Ph. *Solid State Ionics* 1994; **70–71**: 109.
 27. Scanu T, Colomban Ph. *J. Phys. IV* 1993; **C7**: 1927.
 28. Colomban Ph, Lucazeau G, Mercier R, Novak A. *J. Chem. Phys.* 1977; **67**: 5244.
 29. Colomban Ph, Tournié A, Bellot-Gurlet L. *J. Raman Spectrosc.* submitted.
 30. Colomban Ph, Schreiber H. *J. Raman Spectrosc.* 2005; **36**: 884.
 31. Colomban Ph, March G, Mazerolles L, Karmous T, Ayed N, Ennabli A, Slim H. *J. Raman Spectrosc.* 2003; **34**: 205.
 32. Colomban Ph (ed). *Proton Conductors*. Cambridge University Press: Cambridge, 1992.
 33. Colomban Ph. *J. Mol. Struct.* 1992; **270**: 407.
 34. Greaves GN, Fontaine A, Lagarde P, Raoux D, Gurman SJ. *Nature* 1981; **293**: 611.
 35. Carabatos-Nédelec C. Raman scattering of glass. In *Handbook of Raman Spectroscopy*, Lewis IR, Edwards HGM (eds). Marcel Dekker: New York, 2001; Chapt. 10.